RESEARCH ARTICLE | JUNE 20 2023

# The vertical longitudinal magnetoresistance in a van der Waals thin film of $WTe_{_2}$

Y. S. Liu 🛂 📵 ; H. Xiao 📵 ; C. Zhang; C. W. Zhang 🔟 ; Y. G. Shi; T. Hu; C. M. Schneider 🛂 📵



Appl. Phys. Lett. 122, 253101 (2023) https://doi.org/10.1063/5.0151240









## The vertical longitudinal magnetoresistance in a van der Waals thin film of WTe2

Cite as: Appl. Phys. Lett. 122, 253101 (2023); doi: 10.1063/5.0151240 Submitted: 20 March 2023 · Accepted: 6 June 2023 · Published Online: 20 June 2023













Y. S. Liu, <sup>1,2,3,a)</sup> 🕞 H. Xiao, <sup>4</sup> 🕞 C. Zhang, <sup>5</sup> C. W. Zhang, <sup>6</sup> 🕞 Y. G. Shi, <sup>6</sup> T. Hu, <sup>3</sup> and C. M. Schneider <sup>1,2,a)</sup> 🕞



### **AFFILIATIONS**

- <sup>1</sup>Peter Grünberg Institute PGI-6, Forschungszentrum Jülich, D-52425 Jülich, Germany
- <sup>2</sup>Fakultät für Physik, Universität Duisburg-Essen, D-47057 Duisburg, Germany
- <sup>3</sup>Beijing Academy of Quantum Information Sciences, Beijing 100193, China
- <sup>4</sup>Center for High Pressure Science and Technology Advanced Research, Beijing 100094, China
- $^{5}$ State Key Laboratory of Functional Materials for Informatics, Shanghai Institute of Microsystem and Information Technology, Chinese Academy of Sciences, Shanghai 200050, China
- <sup>6</sup>Institute of Physics, Chinese Academy of Sciences, Beijing 100190, China

#### **ABSTRACT**

We report the magneto-transport measurements of thin film devices of the topological Weyl semimetal WTe2 with the applied current along and vertical to the in-plane directions. The device is composed of a van der Waals thin film of WTe<sub>2</sub> sandwiched between top and bottom Au electrodes. At low temperatures, we observe not only a large unsaturated magnetoresistance and Shubnikov-de Haas oscillations with current in the in-plane direction but also a saturated vertical longitudinal magnetoresistance and quantum oscillations with current in the out-of-plane direction in a thin film of WTe2. Our work provides insight into the origin of the unsaturated magnetoresistance in WTe2 and may inspire non-planar engineering to reach higher integration in spintronics.

Published under an exclusive license by AIP Publishing. https://doi.org/10.1063/5.0151240

WTe2 is a layered transition-metal dichalcogenide (TMD) consisting of a tungsten layer surrounded by two tellurium layers stacked along the z axis. It exhibits an extremely large magnetoresistance (XMR) and shows no sign of saturation in high fields. The XMR in the type-II Weyl semimetal WTe<sub>2</sub> recently stimulates extensive theoretical and experimental magneto-transport investigations.<sup>2-6</sup> ARPES experiment in WTe2 suggests that the XMR is attributed to the compensation between the balanced electron and hole populations,<sup>6</sup> like the behavior expected in a perfectly compensated semimetal. In contrast to the normal semimetal, WTe2 is a type-II Weyl semimetal, where Fermi surfaces (FSs) consist of a pair of electron- and holepockets contacting at the Weyl node.<sup>5,8</sup> Shubnikov-de Haas (SdH) oscillations and Seebeck and Nernst measurements support the Fermi surface consisting of two pairs of electron-like and hole-like pockets.2-

With the reduction of thickness, a metal-to-insulator transition is observed in thin WTe2 flakes.9 Gate-tunable magnetoresistance is found in ultra-thin WTe<sub>2</sub>. <sup>10,11</sup> In atomically thin WTe<sub>2</sub>, the magnetoresistance can be tuned from positive to negative. 12 In addition, by electrostatically doping ultra-thin WTe2, the XMR is turned on and off. 13 In a monolayer crystal WTe<sub>2</sub>, the quantum spin Hall effect 14 and

Landau quantization<sup>15</sup> are observed. In bilayers of WTe<sub>2</sub>, the nonlinear Hall effect is observed in spite of its non-magnetic and time-reversal-symmetric conditions.<sup>16</sup> It needs further investigation in the WTe<sub>2</sub> ultra-thin flake, where the electronic structure is modulated by the dimension.1

In this paper, we fabricate a thin film device of WTe<sub>2</sub> with top and bottom electrode structures. By choosing the current directions, we performed anisotropic magneto-transport measurements in this device. We found a large unsaturated magnetoresistance with current in the in-plane direction and a saturated vertical longitudinal magnetoresistance. The Shubnikov-de Haas oscillations are also observed in the magnetoresistance at both directions at low temperature.

Single crystals of WTe2 were synthesized using a self-flux method. WTe2 thin flake was transferred with the polyvinyl alcohol (PVA), based on our previous technique. 18 Figure 1 shows the schematics of the vertical contact fabrication and assembly process comprised of the following steps: (a) the electrodes are patterned when the mask is exposed to UV light. (b) Gold is deposited to the SiO<sub>2</sub>/Si substrate and the residual photoresist is removed with a standard liftoff process as depicted. (c) PVA solution was spin-coated on the SiO<sub>2</sub>/Si

<sup>&</sup>lt;sup>a)</sup>Authors to whom correspondence should be addressed: liuys@baqis.ac.cn and c.m.schneider@fz-juelich.de

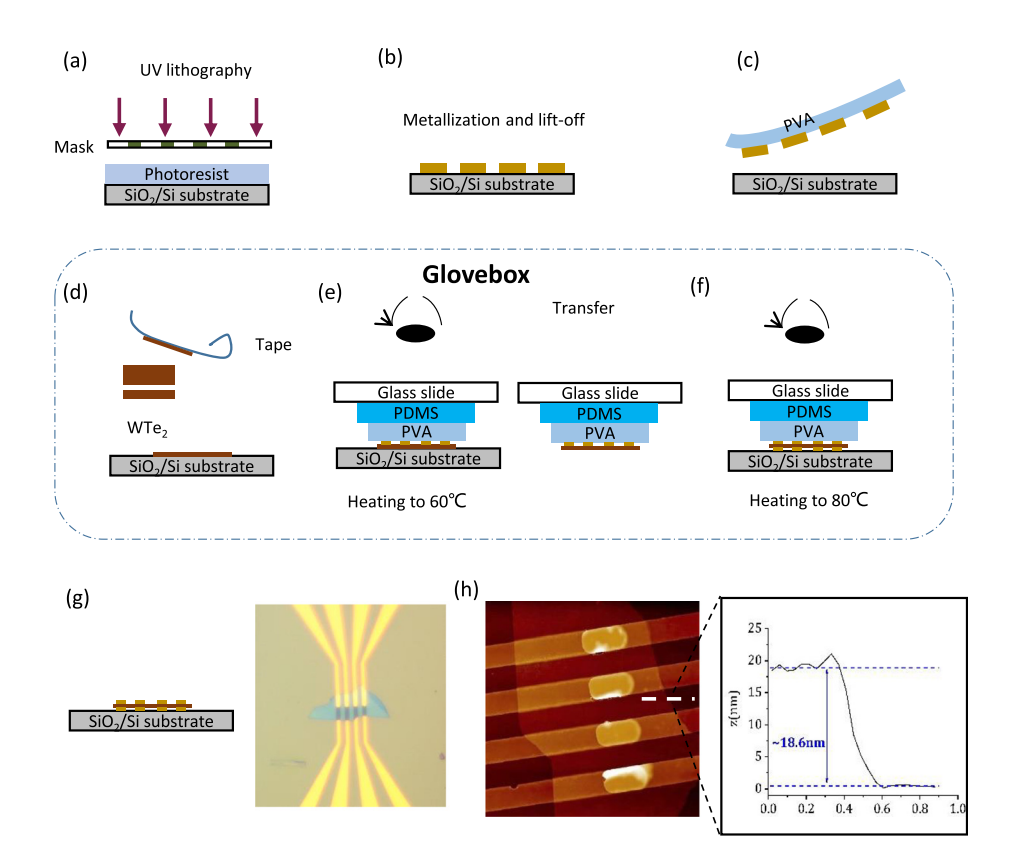


FIG. 1. Schematics of the fabrication process. (a) UV lithography patterning onto the SiO<sub>2</sub>/Si substrate. (b) Au is deposited onto the SiO2/Si substrate, and Au electrodes are left after a standard liftoff process applied to remove the photoresist. (c) The Au electrodes are peeled off by polyvinyl alcohol (PVA) at room temperature from the SiO<sub>2</sub>/Si substrate. (d) Preparation of exfoliated WTe2 flake on the SiO<sub>2</sub>/Si substrate in glovebox. (e) The Au/PVA/PDMS prepared on glass slide are in contact with the thin WTe2 film when heating the stage to 60 °C. After heated for 2 min, the WTe2/Au/PVA/PDMS structure is obtained after gentle separation of the glass slide from the SiO2/Si substrate. (f) Adjusting the relative position of Au electrodes on the SiO2/Si substrate and WTe2/Au/PVA/PDMS on glass slide under an optical microscope and make gentle contact. The stage is kept heating to 80 °C for 2 min. (g) After gentle separation from the PDMS on the glass slide, the Au-electrodes/WTe2/Au-electrodes device is obtained. Schematic structure and optical image of the device are shown. (h) AFM micrograph of fabricated WTe2 vertical structures shows the vertical channel region. Height profile (right inset) is extracted along the dotted line.

substrate with Au electrodes at a speed of 4000 rpm. It created a PVA film of about 900 nm. After 12 h in atmosphere, the PVA becomes dry and solid. At room temperature, the Au electrodes are gently peeled off from the SiO<sub>2</sub>/Si substrate by PVA. 18,19 (d) The WTe<sub>2</sub> thin flakes can be exfoliated using scotch tapes and attached to the SiO2/Si substrate prior to plasma cleaning. (e) A piece of the Au/PVA strip is attached to the Polydimethylsiloxane (PDMS) and glass slide, under the microscope, they are aligned to the thin sample flake. After a short baking of 60 °C, the sample can be gently separated from the substrate and grabbed by the PVA side. (f) We align the Au electrodes part on the SiO<sub>2</sub>/Si substrate with the WTe<sub>2</sub>/Au/PVA/PDMS part on the glass slide under the microscope. After a short baking of 80 °C, the top PDMS is detached. (g) After the PVA is washed away in de-ionized water and the part left is a Au/WTe2/Au vertical structure on the SiO2/ Si substrate. The optical microscope image of the vertical device is shown in the right part. Atomic force microscopy (AFM), Fig. 1(h), reveals the vertical channel region (in bright yellow color) of the device. The width of the vertical channel is about 3  $\mu$ m, and the height profile in the inset shows that the thickness of the WTe2 flake is 18.6 nm, approximately 26 layers taking account of the monolayer 0.7 nm.

Figure 2(a) shows the scanning electron micrograph (SEM) of the WTe<sub>2</sub> van der Waals device. The thin flake of WTe<sub>2</sub> is sandwiched between Au electrodes. The top and bottom Au electrodes are laterally edge-to-edge separated by 3  $\mu$ m from each other, respectively. The mismatch among top and bottom electrodes is inspected by the magnified area in the inset. The mismatch length (d<sub>s</sub>) is about 0.69 and 0.72  $\mu$ m, with a small inclination of about 4.3%. The device can be

used for measuring the planar and vertical transport properties at the same sample. For the in-plane transport configuration, the electrodes 5 and 8 are used as current probes and inner electrodes 6 and 7 are connected to a voltmeter. While for vertical longitudinal transport configuration, the electrodes 2 and 6 are used as current probes and the electrodes 3 and 7 as voltage probes. The resistance was measured by two sets of lock-in amplifiers Stanford SR830 in a 14 T Oxford instrument Teslatron PT. To avoid the influence of noise from different directions, the vertical longitudinal transport measurements were performed subsequently after the in-plane measurements. In our measurement, the four probe resistances for  $R_{ab}$  and  $R_c$  measured at 300 K were 45.7 and 0.66  $\Omega$ , respectively.

Figures 2(b) and 2(c) show the temperature (T) dependence of the normalized resistances ( $R_{ab}$  and  $R_c$ ) at the same WTe<sub>2</sub> sample under the perpendicular external magnetic fields and the applied current (I) along the in-plane and the out-of-plane directions, respectively. It is found that the  $R_{ab}$  at 0 T decreases monotonically from room temperature as the temperature cools down, yielding a residual resistivity ratio (RRR) about 12.5 in Fig. 2(b). The  $R_{ab}$  shows a remarkable increase after reaching a minimum at the turn-on temperature, when a magnetic field is applied. The turn-on temperature is found to be shifted to a higher temperature as increasing H at the investigated magnetic field range. On the other hand, the RRR for  $R_c$  at 0 T is about 6.4 [Fig. 2(c)], which is less than the one for  $R_{ab}$ . Furthermore, the  $R_c$  shows a negligible increase at low temperature at the investigated  $H \leq 14$  T. It, therefore, suggests that the in-plane and out-of-plane transport have distinct electronic properties.

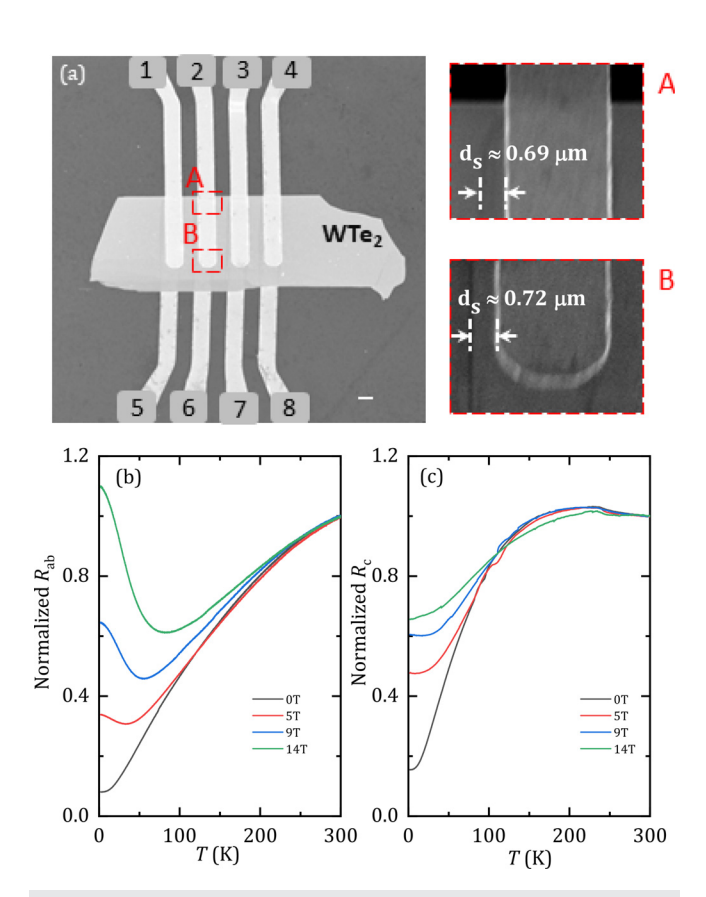


**FIG. 2.** Structure and transport behavior of the WTe<sub>2</sub> device. (a) Scanning electron micrographs of the WTe<sub>2</sub> device, consisting of the ultrathin WTe<sub>2</sub> film sandwiched between the top (marked with 1, 2, 3, and 4) and bottom (marked with 5, 6, 7, and 8) gold electrodes. The scale bar is 3  $\mu$ m. The mismatch between the top and bottom electrodes is about  $0.69~\mu$ m for the region A in the enlarged area while about  $0.72~\mu$ m for the region B. The normalized resistance R(T)/R(300~K) vs T with the current along ab (b) and c directions (c), respectively, under various magnetic fields H parallel to the c axis.

Figure 3(a) shows the *H* dependence of the in-plane magnetoresistance (MR<sub>ab</sub>) at various temperatures (T). The MR<sub>ab</sub> increases with H without a sign of saturation, consistent with the literature.  $^{1,3,20-22}$  At high H, the Shubnikov-de Haas quantum oscillations are observed in all the temperatures from 1.6 to 10 K. The oscillatory component can be extracted by subtracting a second-order polynomial background over the MR. The  $\Delta R_{ab}/R_{ab}(H)$  as a function of 1/H is plotted in Fig. 3(b). Fast Fourier transformation (FFT) has been performed, and the amplitude spectra are illustrated in Fig. 3(c). The frequencies of the thin flake show four major peaks at 77.8, 100, 133, and 161 T, originated from two pairs of electrons and hole pockets.<sup>2,3,5</sup> The decrease and shift of the SdH oscillation frequencies are due to the spatial confinement contributing to the electronic structure in thin samples.<sup>5,17</sup> In addition to the four distinct frequencies, a fifth frequency ( $P_5 = 254 \text{ T}$ ) is detected. It is externally caused by the magnetic breakdown as suggested by a previous study.<sup>2,3</sup> The peaks correspond to the orthogonal cross-sectional area of the Fermi surface (FS)  $A_F$ , as described by the Onsager relation  $F = (\Phi_0/2 \pi^2) A_F$ , where  $\Phi_0$  is the flux quantum. The effective cyclotron mass of carriers at the observed Fermi surface sheets is evaluated from the temperature dependence of normalized FFT amplitude using the Lifshitza–Kosevich (LK) formula,

FFTamp. 
$$\propto \frac{\alpha m^* T/H}{\sinh(\alpha m^* T/H)}$$
,

where  $\alpha = 2\pi^2 K_B/e\hbar$  and  $m^* = m/m_e$  is the effective mass. Normalized FFT amplitudes of the four peaks for the MR<sub>ab</sub> as a function of T are plotted in Fig. 3(d). Their effective masses are estimated to be 0.266 $m_e$ , 0.206 $m_e$ , 0.278 $m_e$ , and 0.446 $m_e$  for oscillation peaks P<sub>1</sub>, P<sub>2</sub>, P<sub>3</sub>, and P<sub>4</sub>, respectively.

When the current is applied through the vertical channel, we can probe the vertical longitudinal magnetoresistance transport properties in one single sample. The H dependences of  $MR_c$  under different T are shown in Fig. 3(e). The MR<sub>c</sub> at 1.6 K increases with H and saturates at large magnetic field, which is different with MR<sub>ab</sub> of WTe<sub>2</sub>. Since in the in-plane current configuration, the magnetoresistance of WTe<sub>2</sub> increases significantly with magnetic field without saturating,<sup>2,23</sup> the mismatch or lateral component should not lead to a non-monotonic and saturated out-of-plane MR. The MRc shows oscillations at the temperature range from 1.6 to 15 K but then disappear at higher temperatures. Similar to the MR<sub>ab</sub>, the oscillatory component of MR<sub>c</sub> is obtained after a background subtraction, and  $\delta R_c/R_c(H)$  is periodic with 1/H as shown in Fig. 3(f). The resistance in the two directions is mainly limited by the geometry if  $\rho_{ab}$  and  $\rho_c$  are comparable in quantity. Since the current channel length is different, it is  $3 \mu m$  for in-plane resistance while 18.6 nm for the out-of-plane resistance, the out-of-plane resistance is much smaller than the in-plane resistance in our measurement. Thus, the resolution of quantum oscillation is worse in the out-of-plane direction. We observe a weak peak  $Q_1 = 66.7 \, \mathrm{T}$ and an obvious sharp peak  $Q_2 = 106 \,\mathrm{T}$  for the MR<sub>c</sub> in Fig. 3(g). According to the previous reports in the bulk sample, the observed frequencies with out-of-plane current are around those with in-plane current.<sup>3,24</sup> The frequency Q<sub>2</sub> is similar to the P<sub>2</sub>, in agreement with the literature. After a fitting with the normalized amplitude A<sub>o</sub> the effective masses are estimated to be  $0.124m_e$  and  $0.143m_e$  [Fig. 3(h)], smaller than those obtained from the in-plane direction transport measurements.

In addition to the in-plane oscillation, we discover the quantum oscillation in the out-of-plane magnetoresistance. One possible interpretation would be that the Fermi arcs on the top and the bottom surface contribute to a novel type of quantum oscillation phenomena.<sup>24</sup> However, the underlying origin needs further experimental evidence and theoretical analysis. In bulk WTe2, the resistivity first increases with magnetic field at low magnetic field before it starts oscillating with a damping out-of-plane magnetoresistance.<sup>24</sup> However, no sign of saturation is observed in the bulk. There is no previous report for out-of-plane magnetoresistance in WTe2 thin films. The quantum oscillation appears in the suppressed magnetoresistance in the ultrathin film, consistent with the bulk, while it is much more suppressed to saturation. A similar magnetoresistance has been observed in a topological Weyl semimetal TaAs, which has a quadratic field dependent in-plane MR but a negative out-of-plane MR. 26,27 It was interpreted that the electrical current along c direction causes an imbalance of the chemical potentials between the opposite chiral Weyl nodes, which leads to the negative magnetoresistance called as Adler-Bell-Jackiw anomaly.20 Thus, for the topological Weyl semimetal WTe<sub>2</sub>, the saturated or negative out-of-plane magnetoresistance might

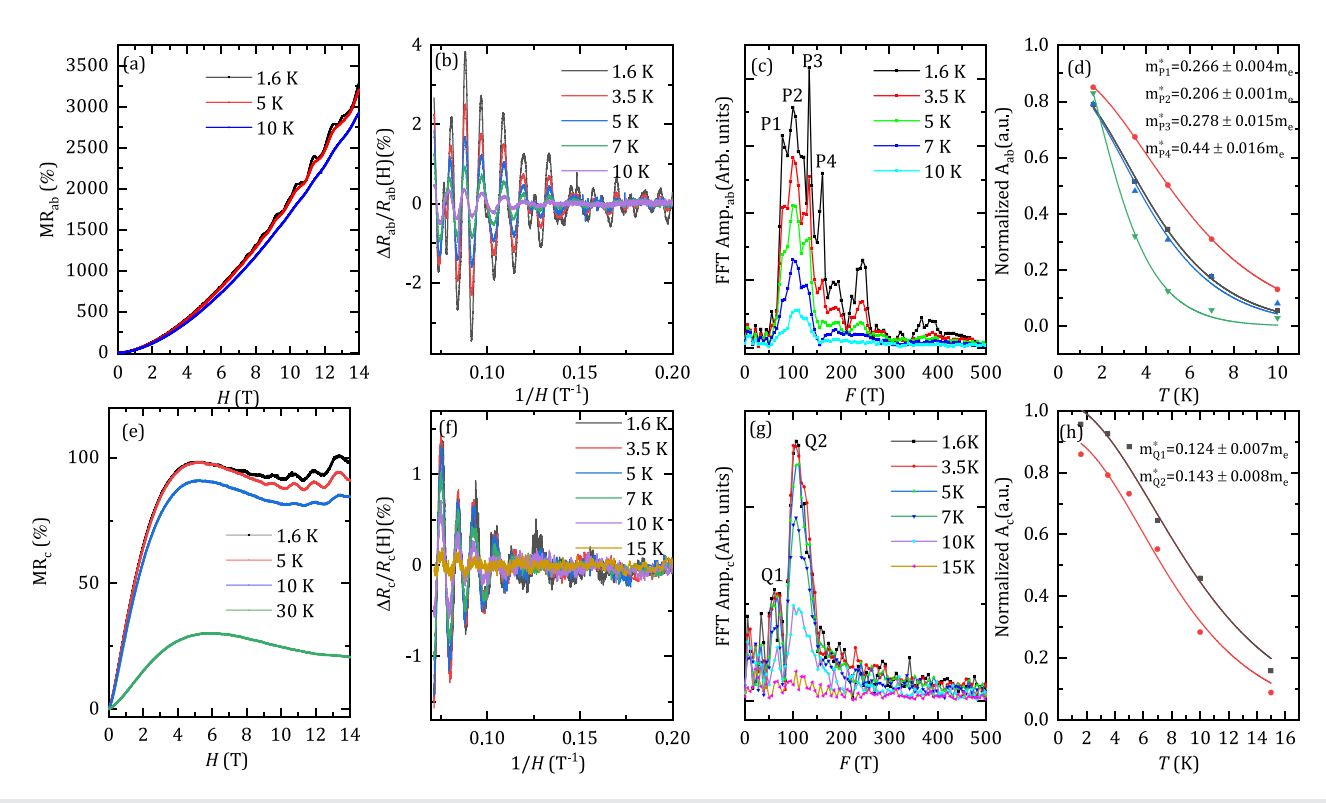


**FIG. 3.** The magneto-transport behaviors in thin film WTe<sub>2</sub>. The H dependence of the magnetoresistance (MR) with the current along ab (a) and c directions (e) at different T. SdH oscillations in MR<sub>ab</sub> (b) and MR<sub>c</sub> (f). The fast Fourier transform (FFT) spectrums of MR<sub>ab</sub> (c) and MR<sub>c</sub> (g). The T dependence of the normalized FFT amplitudes of MR<sub>ab</sub> (d) and MR<sub>c</sub> (h).

be attributed to the electrical current induced Adler-Bell-Jackiw anomaly.

In summary, we introduced the fabrication of the vertically assembled  ${\rm Au/WTe_2/Au/device}$  and characterized its out-of-plane and in-plane transport properties. A saturated out-of-plane magnetoresistance is observed at low temperatures while it remains unsaturated for the in-plane magneto-transport. There are quantum oscillations discovered in the out-of-plane transport in addition to the in-plane transport. Our results suggest that the presence of different behaviors of magnetoresistance could be determined by applied current directions.

T.H. acknowledges the support of NSFC Grant No. 11574338. H.X. acknowledges the support of NSAF Grant No. U1530402. Y. G. Shi acknowledges the support of NSFC Grant No. U2032204 and the Informatization Plan of Chinese Academy of Sciences (No. CAS-WX2021SF-0102).

# AUTHOR DECLARATIONS Conflict of Interest

The authors have no conflicts to disclose.

### **Author Contributions**

**Yinshang Liu:** Conceptualization (equal); Data curation (equal); Formal analysis (equal); Writing – original draft (equal). **Hong Xiao:** Formal

analysis (equal). **Chi Zhang:** Data curation (equal); Formal analysis (equal). **Cuiwei zhang:** Data curation (equal). **Youguo Shi:** Data curation (equal). **Tao Hu:** Data curation (equal); Formal analysis (equal); Writing – review & editing (equal); Supervision (equal). **Claus M. Schneider:** Writing – review & editing (equal); Supervision (equal).

### **DATA AVAILABILITY**

The data that support the findings of this study are available within the article.

#### **REFERENCES**

<sup>1</sup>M. N. Ali, J. Xiong, S. Flynn, J. Tao, Q. D. Gibson, L. M. Schoop, T. Liang, N. Haldolaarachchige, M. Hirschberger, N. P. Ong *et al.*, "Large, non-saturating magnetoresistance in WTe<sub>2</sub>," Nature **514**(7521), 205–208 (2014).

<sup>2</sup>P. L. Cai, J. Hu, L. P. He, J. Pan, X. C. Hong, Z. Zhang, J. Zhang, J. Wei, Z. Q. Mao, and S. Y. Li, "Drastic pressure effect on the extremely large magnetoresistance in WTe<sub>2</sub>: Quantum oscillation study," Phys. Rev. Lett. 115(5), 057202 (2015).

<sup>3</sup>Z. Zhu, X. Lin, J. Liu, B. Fauqué, Q. Tao, C. Yang, Y. Shi, and K. Behnia, "Quantum oscillations, thermoelectric coefficients, and the fermi surface of semimetallic WTe<sub>2</sub>," Phys. Rev. Lett. **114**(17), 176601 (2015).

<sup>4</sup>L. R. Thoutam, Y. L. Wang, Z. L. Xiao, S. Das, A. Luican-Mayer, R. Divan, G. W. Crabtree, and W. K. Kwok, "Temperature-dependent three-dimensional anisotropy of the magnetoresistance in WTe<sub>2</sub>," Phys. Rev. Lett. 115(4), 046602 (2015).

<sup>5</sup>P. Li, Y. Wen, X. He, Q. Zhang, C. Xia, Z.-M. Yu, S. A. Yang, Z. Zhu, H. N. Alshareef, and X.-X. Zhang, "Evidence for topological type-II Weyl semimetal WTe<sub>2</sub>," Nat. Commun. 8(1), 2150 (2017).

- <sup>6</sup>I. Pletikosić, M. N. Ali, A. V. Fedorov, R. J. Cava, and T. Valla, "Electronic structure basis for the extraordinary magnetoresistance in WTe<sub>2</sub>," Phys. Rev. Lett. 113(21), 216601 (2014).
- <sup>7</sup>A. B. Pippard, Magnetoresistance in Metals (Cambridge University Press, 1989), Vol. 2.
- <sup>8</sup>A. A. Soluyanov, D. Gresch, Z. Wang, Q. Wu, M. Troyer, X. Dai, and B. A. Bernevig, "Type-II Weyl semimetals," Nature 527(7579), 495–498 (2015).
- <sup>9</sup>L. Wang, I. Gutiérrez-Lezama, C. Barreteau, N. Ubrig, E. Giannini, and A. F. Morpurgo, "Tuning magnetotransport in a compensated semimetal at the atomic scale," Nat. Commun. 6(1), 8892 (2015).
- <sup>10</sup>Y. Wang, E. Liu, H. Liu, Y. Pan, L. Zhang, J. Zeng, Y. Fu, M. Wang, K. Xu, Z. Huang *et al.*, "Gate-tunable negative longitudinal magnetoresistance in the predicted type-II Weyl semimetal WTe<sub>2</sub>," Nat. Commun. 7(1), 13142 (2016).
- <sup>11</sup>X. Liu, Z. Zhang, C. Cai, S. Tian, S. Kushwaha, H. Lu, T. Taniguchi, K. Watanabe, R. J. Cava, S. Jia *et al.*, "Gate tunable magneto-resistance of ultrathin WTe<sub>2</sub> devices," 2D Mater. 4(2), 021018 (2017).
- <sup>12</sup>E. Zhang, R. Chen, C. Huang, J. Yu, K. Zhang, W. Wang, S. Liu, J. Ling, X. Wan, H.-Z. Lu *et al.*, "Tunable positive to negative magnetoresistance in atomically thin WTe<sub>2</sub>," Nano Lett. 17(2), 878–885 (2017).
- <sup>13</sup>V. Fatemi, Q. D. Gibson, K. Watanabe, T. Taniguchi, R. J. Cava, and P. Jarillo-Herrero, "Magnetoresistance and quantum oscillations of an electrostatically tuned semimetal-to-metal transition in ultrathin WTe<sub>2</sub>," Phys. Rev. B 95(4), 041410 (2017).
- <sup>14</sup>S. Wu, V. Fatemi, Q. D. Gibson, K. Watanabe, T. Taniguchi, R. J. Cava, and P. Jarillo-Herrero, "Observation of the quantum spin hall effect up to 100 kelvin in a monolayer crystal," Science 359(6371), 76–79 (2018).
- <sup>15</sup>P. Wang, G. Yu, Y. Jia, M. Onyszczak, F. A. Cevallos, S. Lei, S. Klemenz, K. Watanabe, T. Taniguchi, R. J. Cava et al., "Landau quantization and highly mobile fermions in an insulator," Nature 589(7841), 225–229 (2021).
- <sup>16</sup>Q. Ma, S.-Y. Xu, H. Shen, D. MacNeill, V. Fatemi, T.-R. Chang, A. M. Mier Valdivia, S. Wu, Z. Du, C.-H. Hsu *et al.*, "Observation of the nonlinear Hall effect under time-reversal-symmetric conditions," Nature 565(7739), 337–342 (2019).
- <sup>17</sup>F.-X. Xiang, A. Srinivasan, Z. Z. Du, O. Klochan, S.-X. Dou, A. R. Hamilton, and X.-L. Wang, "Thickness-dependent electronic structure in WTe<sub>2</sub> thin films," Phys. Rev. B 98(3), 035115 (2018).

- <sup>18</sup>C. Zhang, T. Hu, T. Wang, Y. Wu, A. Yu, J. Chu, H. Zhang, X. Zhang, H. Xiao, W. Peng *et al.*, "Observation of two-dimensional superconductivity in an ultrathin iron–arsenic superconductor," 2D Mater. 8(2), 025024 (2021).
- <sup>19</sup>Y. Cao, X. Wang, X. Lin, W. Yang, C. Lv, Y. Lu, Y. Zhang, and W. Zhao, "Movable-type transfer and stacking of van der Waals heterostructures for spintronics," IEEE Access 8, 70488–70495 (2020).
- <sup>20</sup>W.-D. Kong, S.-F. Wu, P. Richard, C.-S. Lian, J.-T. Wang, C.-L. Yang, Y.-G. Shi, and H. Ding, "Raman scattering investigation of large positive magnetoresistance material WTe<sub>2</sub>," Appl. Phys. Lett. **106**(8), 081906 (2015).
- <sup>21</sup>Y. Zhao, H. Liu, J. Yan, W. An, J. Liu, X. Zhang, H. Wang, Y. Liu, H. Jiang, Q. Li *et al.*, "Anisotropic magnetotransport and exotic longitudinal linear magnetoresistance in WTe<sub>2</sub> crystals," Phys. Rev. B 92(4), 041104 (2015).
- <sup>22</sup>F.-X. Xiang, M. Veldhorst, S.-X. Dou, and X.-L. Wang, "Multiple Fermi pockets revealed by Shubnikov-de Haas oscillations in WTe<sub>2</sub>," Europhys. Lett. 112(3), 37009 (2015).
- <sup>23</sup>M. N. Ali, L. Schoop, J. Xiong, S. Flynn, Q. Gibson, M. Hirschberger, N. P. Ong, and R. J. Cava, "Correlation of crystal quality and extreme magnetoresistance of WTe<sub>2</sub>," Europhys. Lett. 110(6), 67002 (2015).
- <sup>24</sup>R. Bi, Z. Feng, X. Li, J. Niu, J. Wang, Y. Shi, D. Yu, and X. Wu, "Spin zero and large Landé g-factor in WTe<sub>2</sub>," New J. Phys. **20**(6), 063026 (2018).
- 25A. C. Potter, I. Kimchi, and A. Vishwanath, "Quantum oscillations from surface fermi arcs in Weyl and Dirac semimetals," Nat. Commun. 5(1), 5161 (2014).
- 26B. J. Ramshaw, K. A. Modic, A. Shekhter, Y. Zhang, E.-A. Kim, P. J. Moll, M. D. Bachmann, M. K. Chan, J. B. Betts, F. Balakirev et al., "Quantum limit transport and destruction of the Weyl nodes in TaAs," Nat. Commun. 9(1), 2217 (2018).
- <sup>27</sup>X. Huang, L. Zhao, Y. Long, P. Wang, D. Chen, Z. Yang, H. Liang, M. Xue, H. Weng, Z. Fang *et al.*, "Observation of the chiral-anomaly-induced negative magnetoresistance in 3D Weyl semimetal TaAs," Phys. Rev. X 5(3), 031023 (2015).
- <sup>28</sup>H. B. Nielsen and M. Ninomiya, "The Adler-Bell-Jackiw anomaly and Weyl fermions in a crystal," Phys. Lett. B 130(6), 389–396 (1983).
- <sup>29</sup>S. L. Adler, "Axial-vector vertex in spinor electrodynamics," Phys. Rev. 177(5), 2426 (1969).
- 30 M. E. Peskin and D. V. Schroeder, An Introduction to Quantum Field Theory (Westview Press, Boulder, CO, 1995) Chap. 19.